Supporting Information For

Luminescent and Sublimable Binaphtyl-Based Field-Induced Lanthanide Single-Molecule Magnets

Carlo Andrea Mattei,[a] Thomas Delouche,[a] Bertrand Lefeuvre,[a] Marie Dallon-Cordier,[a] Claudia Lalli,[a] Olivier Cador,[a] Laura Abad Galán,[b] François Riobé,*[b] Olivier Maury,[b] Pierre-Antoine Bouit,*[a] Fabrice Pointillart*[a]

[a] *Univ Rennes, CNRS, ISCR (Institut des Sciences Chimiques de Rennes) – UMR 6226, 35000 Rennes (France)*

*E-mail:*pierre-antoine.bouit@univ-rennes1.fr, fabrice.pointillart@univ-rennes1.fr

[b] *Univ Lyon, ENS de Lyon, CNRS UMR 5182, Laboratoire de Chimie, 69342, Lyon (France)*

E-mail: francois.riobe@ens-lyon.fr

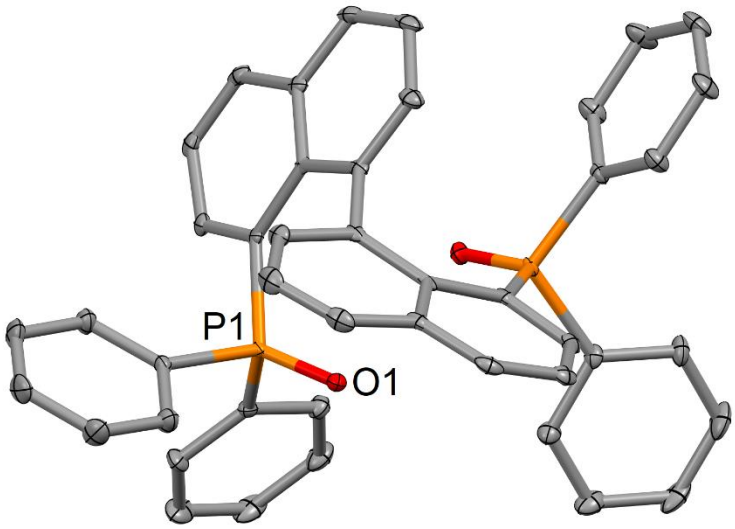

Figure S1. ORTEP view of the asymmetric unit for **L**. Thermal ellipsoids are drawn at 30% probability. Hydrogen atoms are omitted for clarity.

Analytical chiral HPLC separation

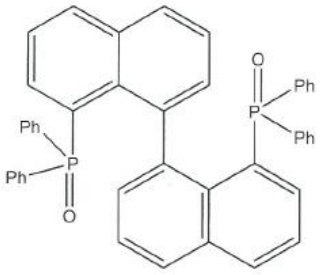

• **L** is dissolved in dichloromethane, injected on the chiral column, and detected with an UV detector at 280 nm and a circular dichroism detector at 254 nm. The flow-rate is 1 mL/min.

Column	Mobile Phase	t1	k1	t2	k2	α	Rs
(*S,S*)-Whelk-O1	Heptane / ethanol / dichloromethane (60/20/20)	4.29 (-)	0.45	5.73 (+)	0.94	2.08	5.71

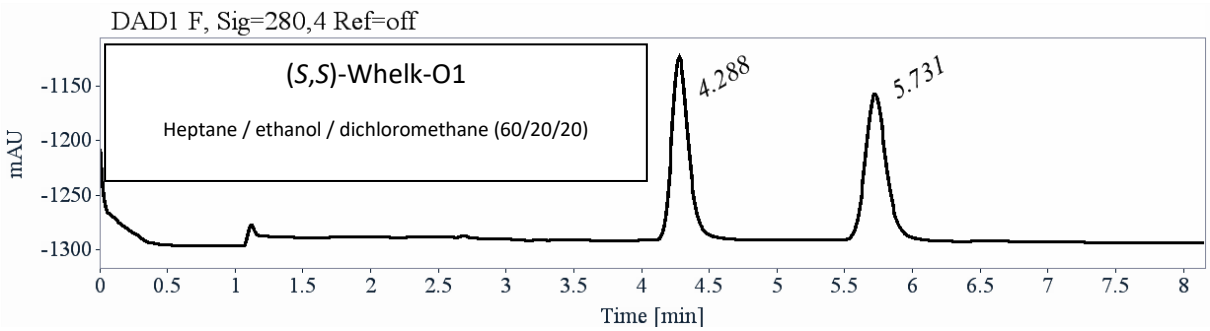

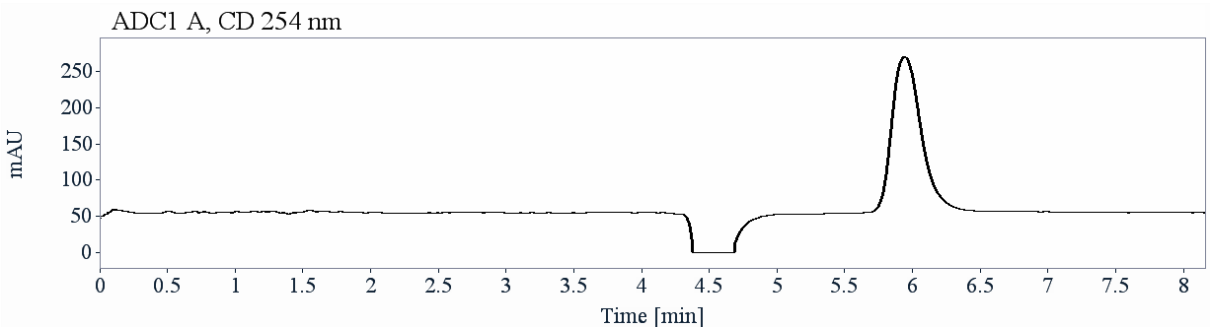

RT [min]	Area	Area%	Capacity Factor	Enantioselectivity	Resolution (USP)
4.29	1485	50.15	0.45		
5.73	1476	49.85	0.94	2.08	5.71
Sum	2960	100.00			

Preparative separation for compound **L**:

• Sample preparation: About 80 mg of compound **L** are dissolved in 5 mL of a mixture of dichloromethane and hexane (60/40). During the preparative separation and the treatment, the collected fractions were ***kept cold, below 10°C***.

• Chromatographic conditions: (*S,S*)-Whelk-O1 (250 x 10 mm), Hexane / ethanol / CH_2Cl_2 (60/20/20) as mobile phase, flow-rate = 5 mL/min, UV detection at 280 nm.

• Injections (stacked): 25 times 200 µL, every 4 minutes.

• First fraction: 35 mg of the first eluted ((-, CD254)-enantiomer) with ee > 93.5%

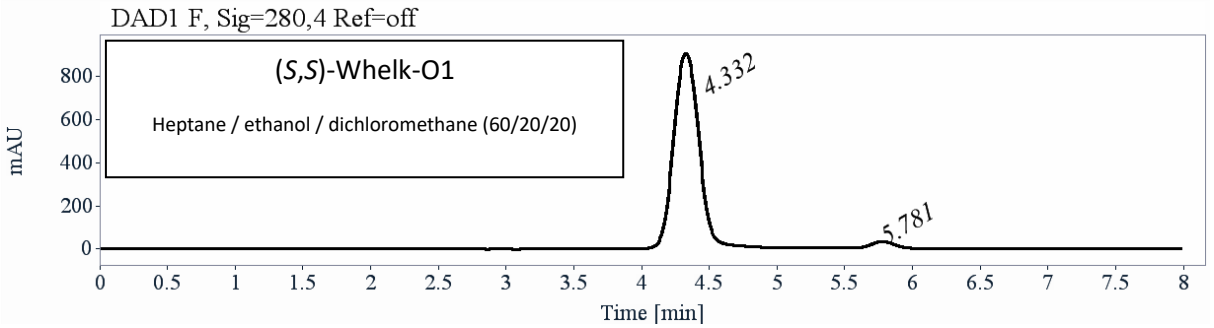

RT [min]	Area	Area%
4.33	11649	96.81
5.78	384	3.19
Sum	12033	100.00

• Second fraction: 33 mg of the second eluted ((+, CD254)-enantiomer) with ee > 94%

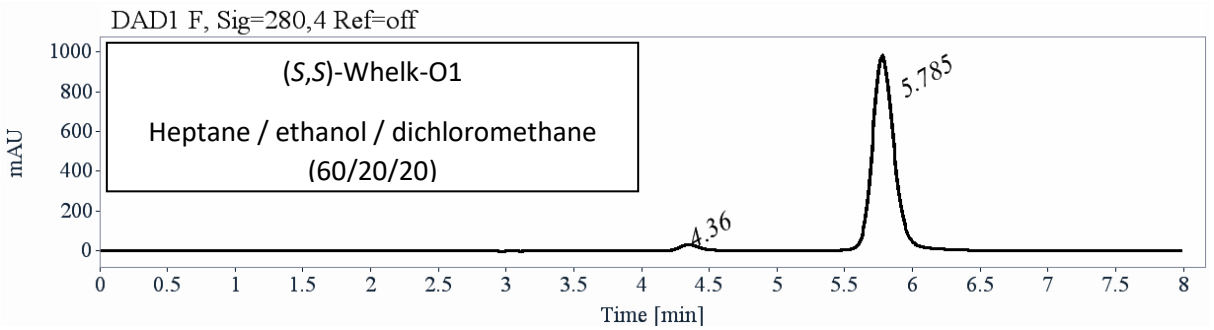

RT [min]	Area	Area%
4.36	314	2.80
5.79	10883	97.20
Sum	11197	100.00

Optical rotations

Optical rotations were measured on a Jasco P-2000 polarimeter with a halogen lamp (589, 578, 546, 436 and 405 nm), in a 10 cm cell, thermostated at 15°C with a Peltier controlled cell holder.

Table S1: Optical rotations of the two enantiomers of L

λ (nm)	**L** First eluted enantiomer on (*S*,*S*)-Whelk-O1 $[\alpha]_\lambda^{15}$ (CH_2Cl_2, c =0.17)	**L** Second eluted enantiomer on (*S*,*S*)-Whelk-O1 $[\alpha]_\lambda^{15}$ (CH_2Cl_2, c =0.15)
589	+ 63	- 63
578	+ 66	- 66
546	+ 76	- 76
436	+ 167	- 167
405	+ 286	- 287

Electronic Circular Dichroism

ECD and UV spectra were measured on a JASCO J-815 spectrometer equipped with a JASCO Peltier cell holder PTC-423 to maintain the temperature at 15.0 ± 0.2°C. A CD quartz cell of 1 mm of optical pathlength was used. The CD spectrometer was purged with nitrogen before recording each spectrum, which was baseline subtracted. The baseline was always measured for the same solvent and in the same cell as the samples. The spectra are presented without smoothing and further data processing. Acquisition parameters: 0.1 nm as intervals, scanning speed 50 nm/min, band width 2 nm, and 3 accumulations per sample.

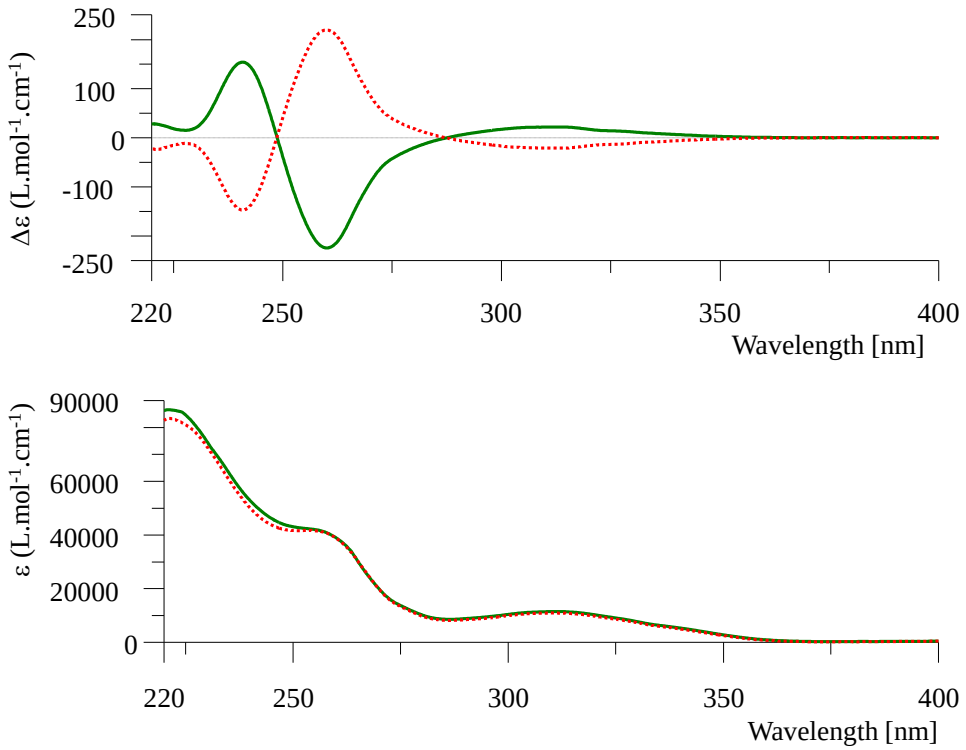

Figure S2: ECD and UV vis absorption spectra of **L**, first eluted enantiomer (green solid line), concentration = 0.123 mmol.L^{-1} I and second eluted enantiomer (red dotted) on (*S*,*S*)-Whelk-O1 in dichloromethane.

Kinetic of enantiomerization of L in Hexane / ethanol / dichloromethane (6/2/2)

The second eluted enantiomer of **L** is thermostated at 30°C and then injected on (S,S)-Whelk-O1 (60:20:20 heptane / ethanol / dichloromethane, 1 mL/min, UV 280 nm). The percentage decrease of the second eluted enantiomer of **L** is monitored.

Time (min)	% second eluted enantiomer	ln ((%t-50%)/(%(t=0)-50%))
0.00	98.5	0.00000
9.55	92.05	-0.14270
19.10	86.02	-0.29749
28.63	80.73	-0.45632
38.17	76.07	-0.62078
47.72	72.06	-0.78780
57.27	68.58	-0.95948

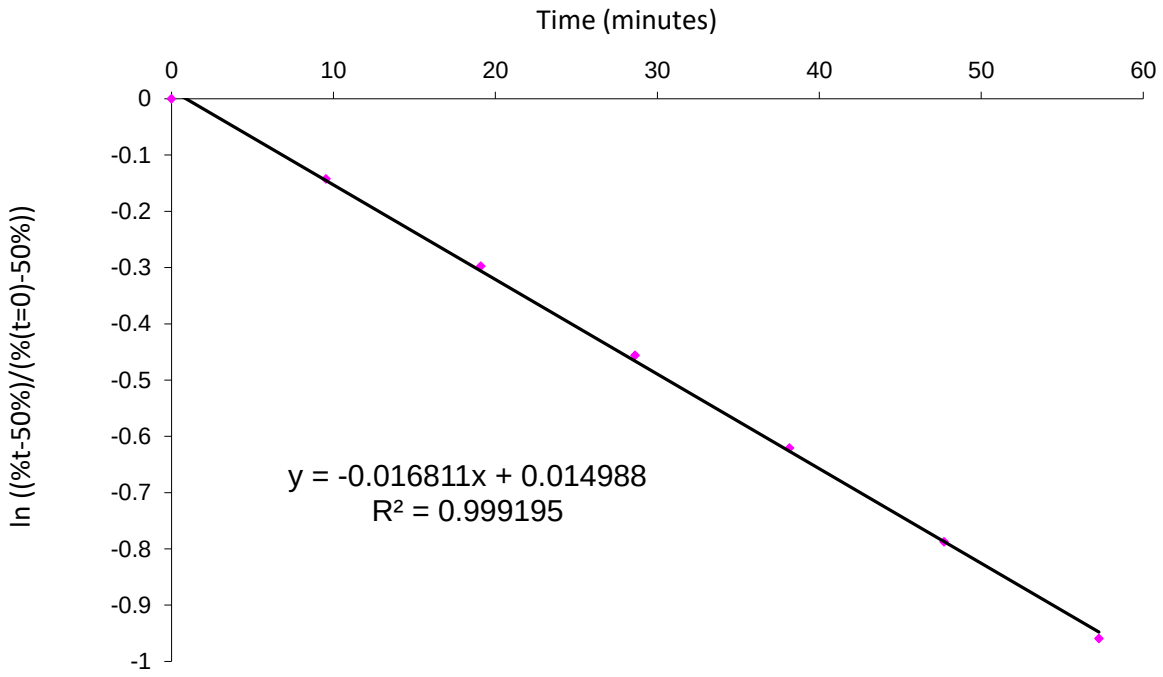

Figure S3: Kinetic of enantiomerization of **L** in Hexane / ethanol / dichloromethane (6/2/2)

$k_{enantiomerisation} = 1.40.10^{-4}\ s^{-1}$ (30°C, Hexane / ethanol / dichloromethane 6:2:2)

$\Delta G^{\neq} = 96.7\ kJ.mol^{-1}$ (30°C, Hexane / ethanol / dichloromethane 6:2:2)

$t_{1/2} = 41$ minutes (30°C, Hexane / ethanol / dichloromethane 6:2:2)

Kinetic of enantiomerization of **L** in dichloromethane

This kinetic study was monitored by electronic circular dichroism. In a CD quartz cell of 1 mm of optical pathlength, 215 µL of a 0.106 mg/mL solution of the second eluted enantiomer of **L** in dichloromethane is thermostated at 30°C. A spectrum (0.1 nm as intervals, scanning speed 50 nm/min, band width 2 nm, 1 accumulation) is recorded every 4 minutes. For each spectrum, the area under the curve between 248 and 288 nm, which is proportional to the enantiomeric excess, is calculated.

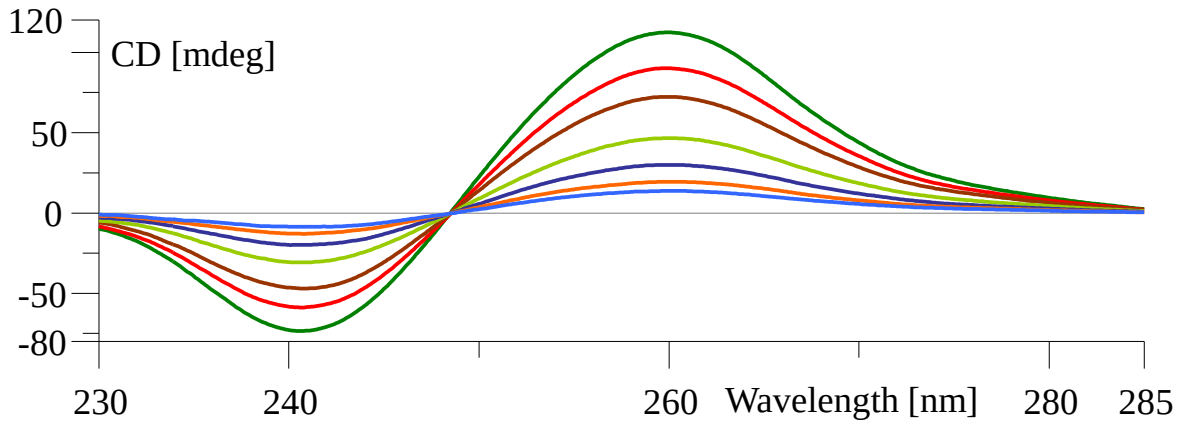

Figure S4. ECD spectra obtained during the racemization along the time for t = 0, 12, 24, 48, 72, 96 and 116 minutes.

Time (min)	Area(t)	ln (Area(t)/Area(0))
0	1897.50	0.0000
4	1762.58	-0.0738
8	1639.33	-0.1462
12	1518.77	-0.2226
16	1414.13	-0.2940
20	1310.41	-0.3702
24	1220.48	-0.4413
28	1132.03	-0.5165
32	1054.58	-0.5874
36	981.90	-0.6588
40	908.92	-0.7360
44	847.53	-0.8060
48	784.69	-0.8830
52	731.93	-0.9526
56	680.52	-1.0254

Time (min)	Area(t)	ln (Area(t)/Area(0))
60	631.61	-1.1000
64	587.55	-1.1723
68	548.50	-1.2411
72	507.42	-1.3189
76	472.12	-1.3911
80	439.38	-1.4629
84	410.81	-1.5302
88	379.14	-1.6104
92	353.21	-1.6812
96	326.34	-1.7603
100	306.53	-1.8230
104	283.99	-1.8994
108	262.25	-1.9790
112	245.51	-2.0450
116	228.51	-2.1167

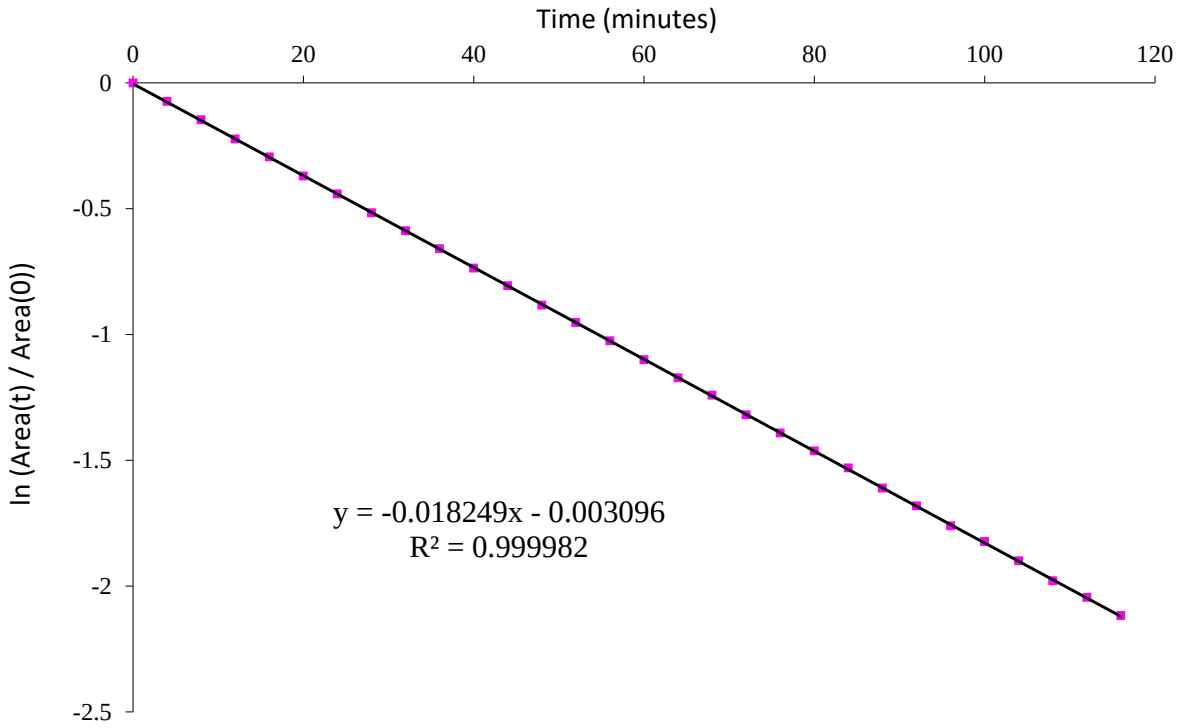

Figure S5: Kinetic of enantiomerization of **L** in dichloromethane.

$k_{enantiomerisation} = 1.52.10^{-4}\ s^{-1}$ (30°C, dichloromethane)

$\Delta G^{\neq} = 96.5\ kJ.mol^{-1}$ (30°C, dichloromethane)

$t_{1/2}$ = 38 minutes (30°C, dichloromethane)

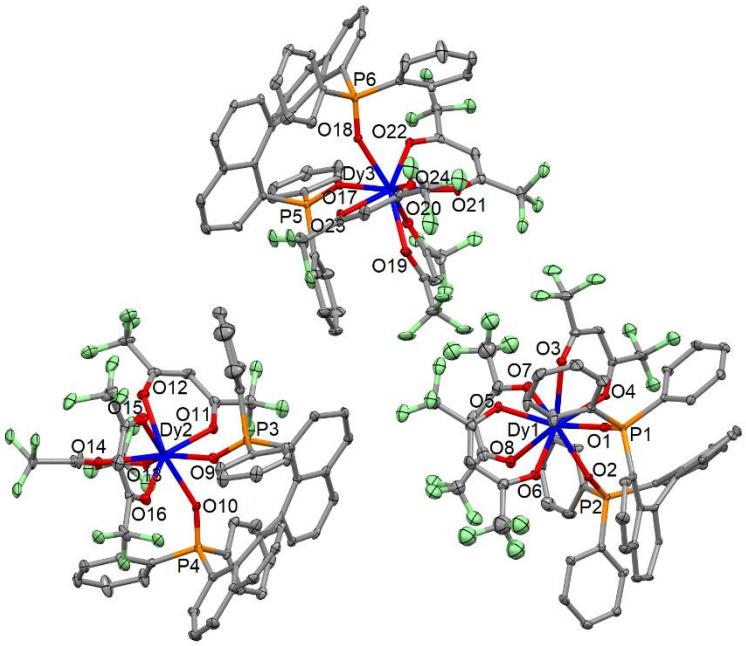

Figure S6. ORTEP view of the asymmetric unit for **1**. Thermal ellipsoids are drawn at 30% probability. Hydrogen atoms are omitted for clarity.

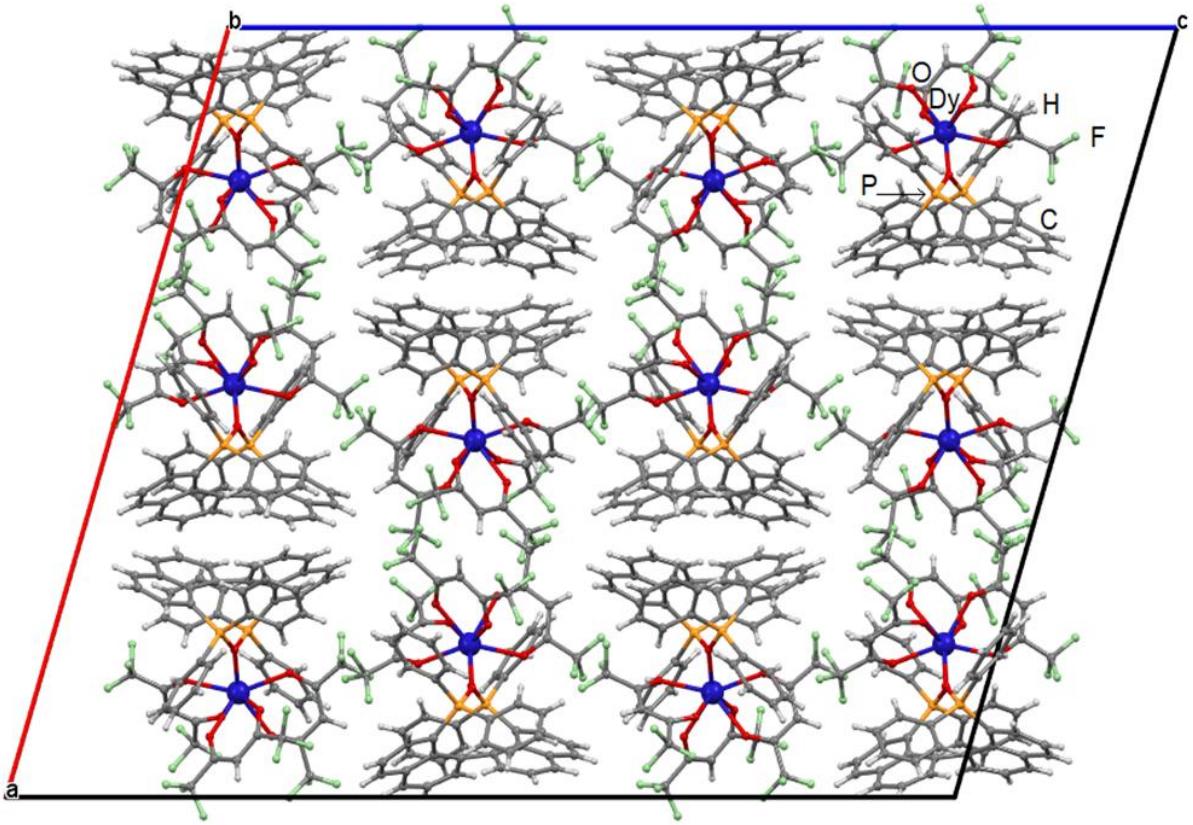

Figure S7. View along the *b* axis of the unit cell for **3**.

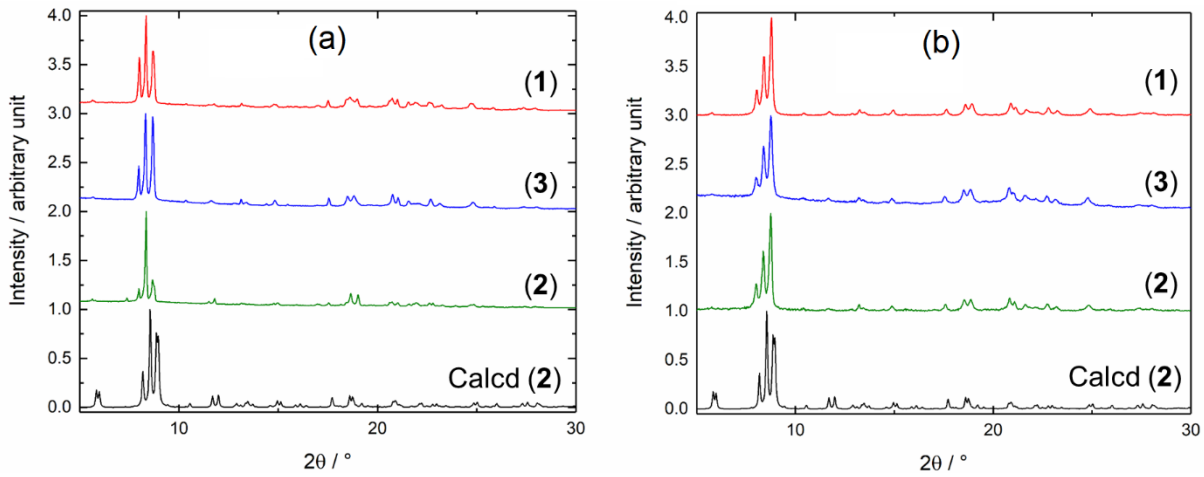

Figure S8. Calculated Powder X-Ray Diffraction (PXRD) diffractogram (black) for the complex **2** and experimental PXRD diffractograms for the species [{Ln(hfac)$_3$**L**}$_3$] with Ln = Eu (**1**) (red), Dy (**2**) (green) and Yb (**3**) (blue) before (a) and after sublimation (b).

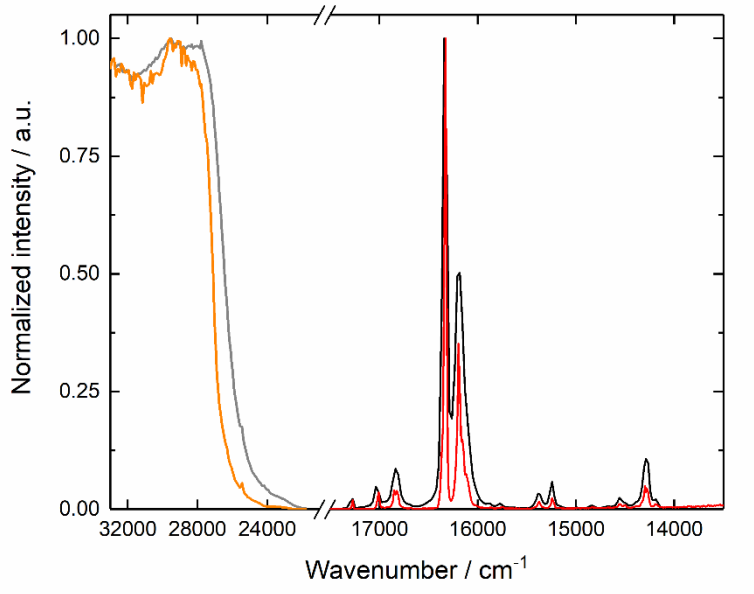

Figure S9. Solid-state excitation spectra of **1** recorded by monitoring the strongest emission (Room temperature and 77 K measurements are depicted in black and in red, respectively). Solid state emission spectra recorded at room temperature (black) and 77 K (red) for **1**.

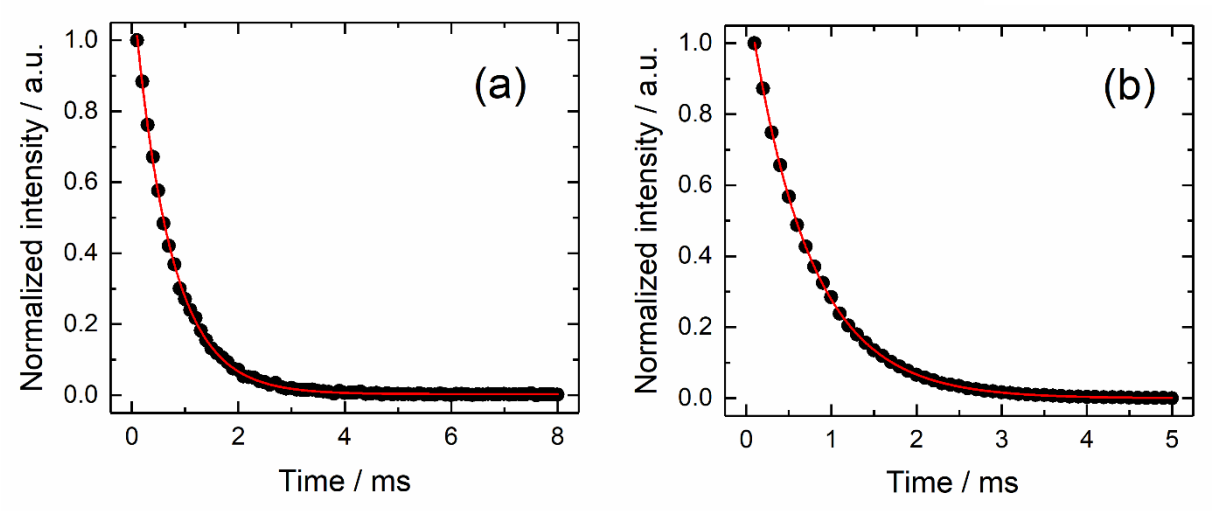

Figure S10. Solid state emission lifetime decays (black dots) at room temperature (a) and 77 K (b) for **1** and mono-exponential decay function fits (red lines).

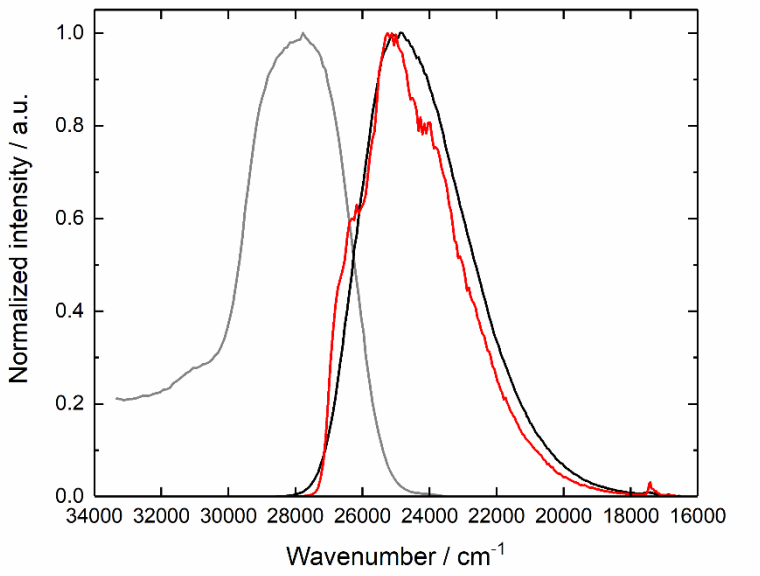

Figure S11. Solid state excitation spectrum recorded at room temperature (grey) and emission spectra recorded at room temperature (black) and 77 K (red) for **2**.

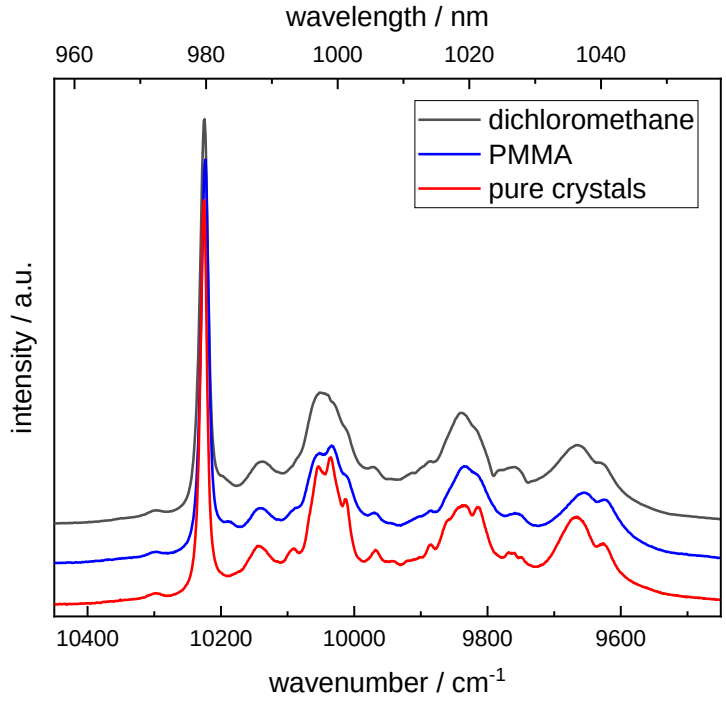

Figure S12. High-resolution emission spectra of **3** at solid state (red) and diluted in a PMMA matrix (blue) or in frozen dichloromethane (black) at 77 K.

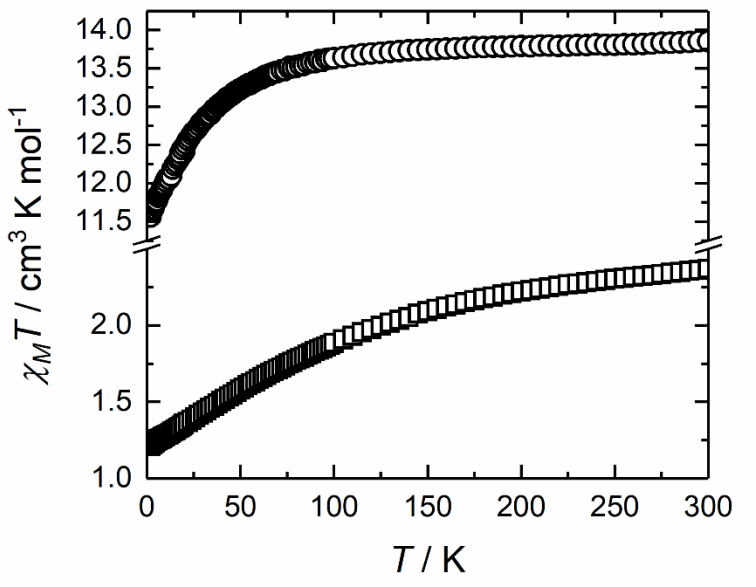

Figure S13. Temperature dependence of the $\chi_M T$ product for **2** (circles) and **3** (squares) for the 2-300 K temperature range.

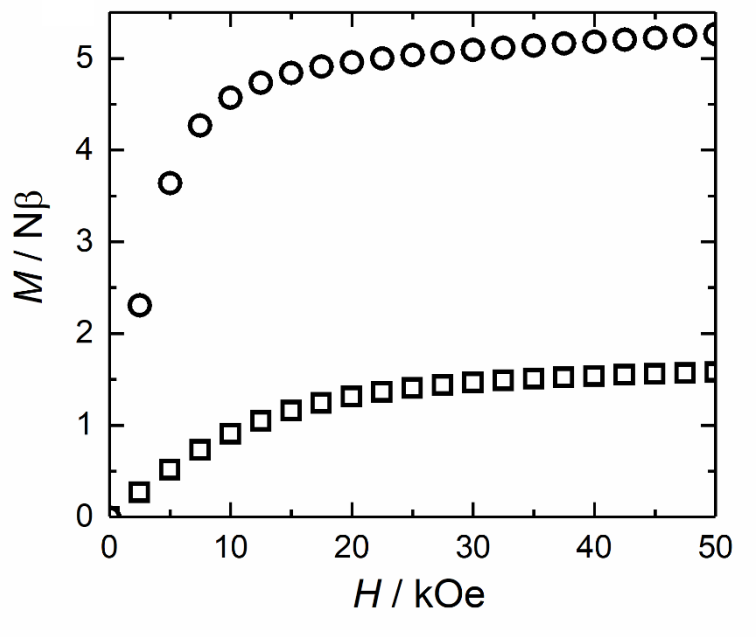

Figure S14. Field variations of the magnetization at 2 K for **2** (circles) and **3** (squares) on the 0-5 T field range.

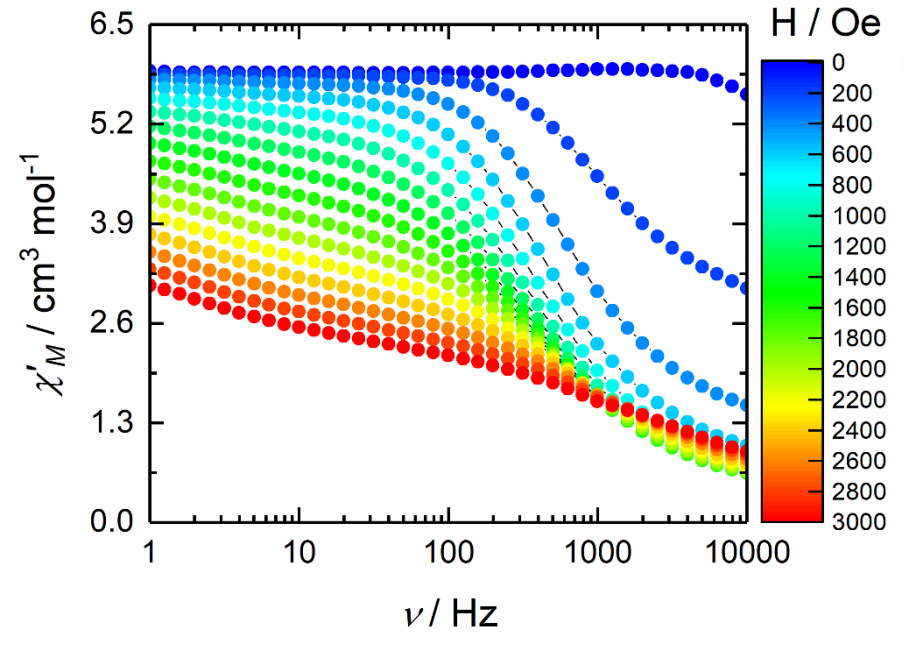

Figure S15. Frequency dependence of χ_M' between 0 and 3000 Oe and at 2 K for **2**.

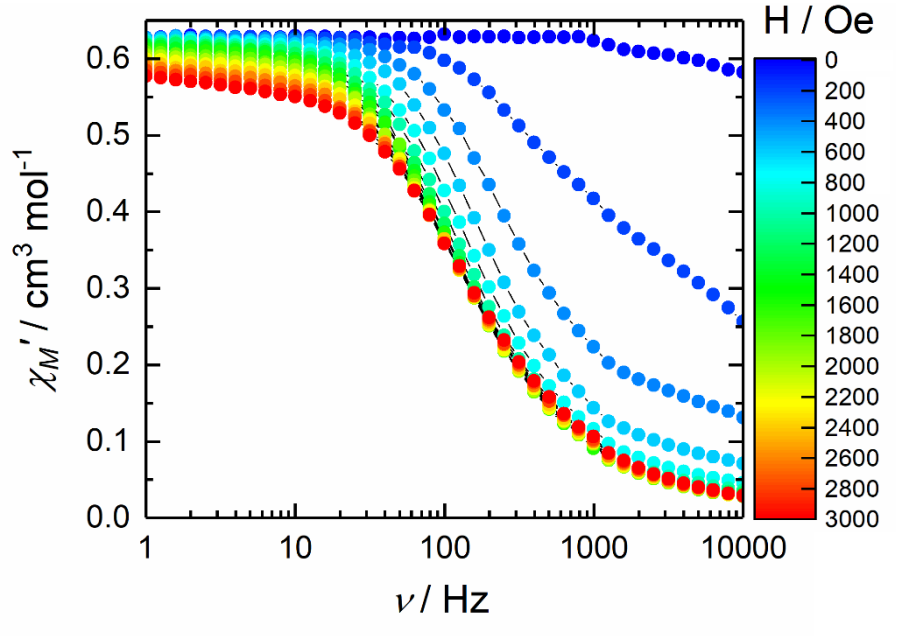

Figure S16. Frequency dependence of χ_M' between 0 and 3000 Oe and at 2 K for **3**.

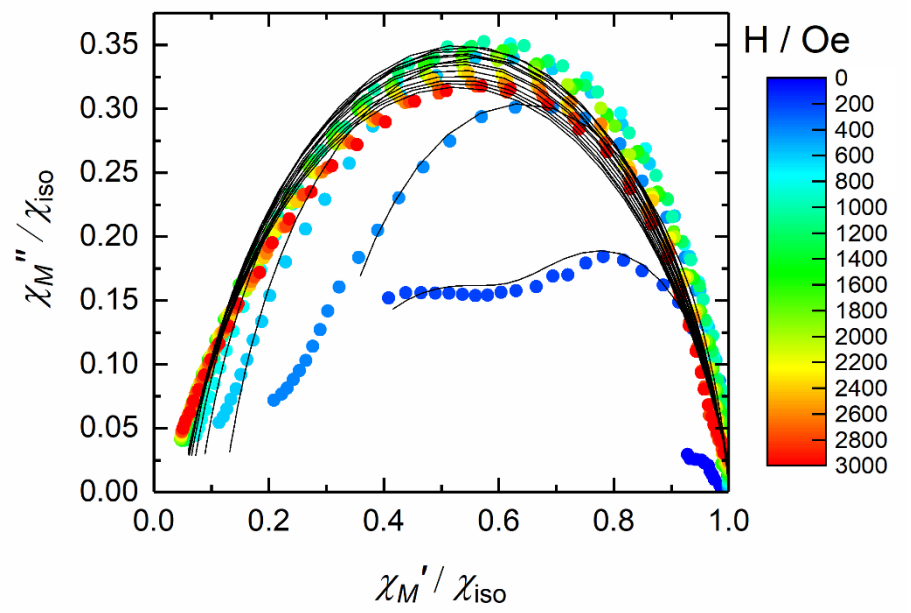

Figure S17. Normalized Argand plot of experimental (colored plots) and fit data (black lines) for **3** at 2 K in the field range 0-3000 Oe.

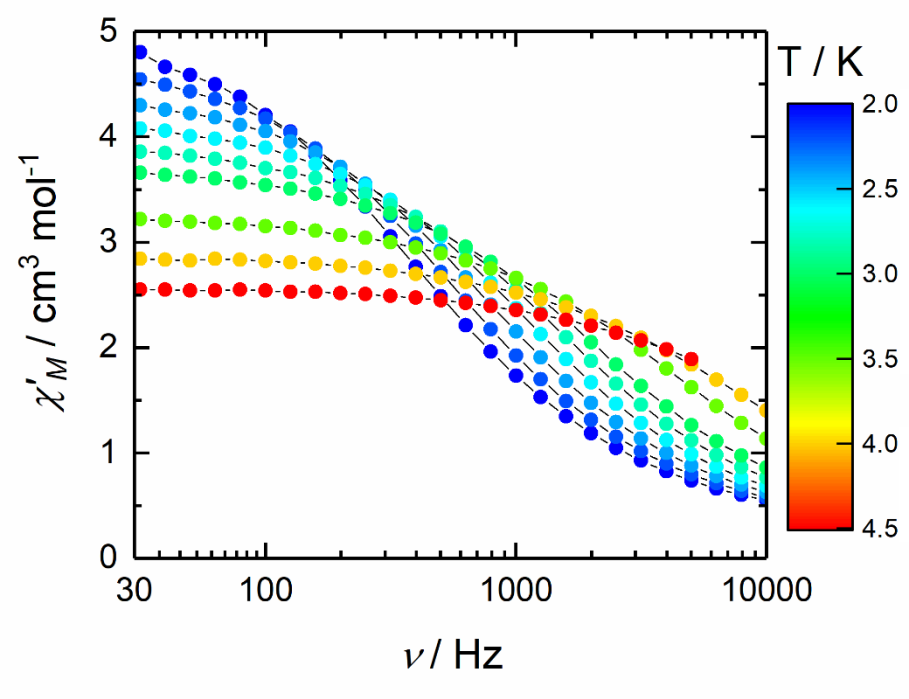

Figure S18. Frequency dependence of χ_M' between 0 and 4.5 K under 800 Oe for **2**.

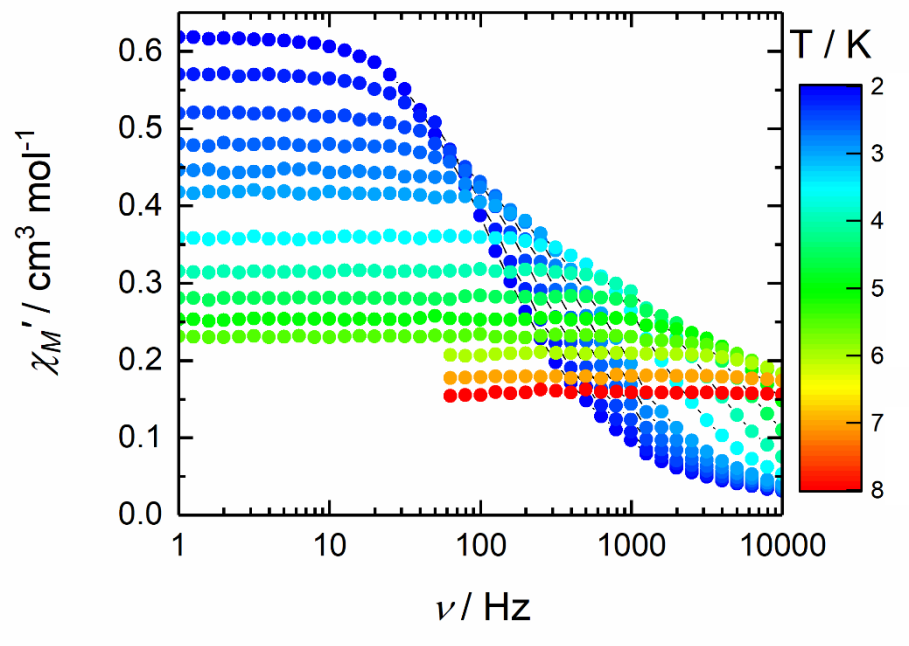

Figure S19. Frequency dependence of χ_M' between 0 and 4.5 K under 1200 Oe for **3**.

Extended Debye model used for magnetic susceptibility with one contribution.

$$\chi_M' = \chi_S + (\chi_T - \chi_S)\frac{1+(\omega\tau)^{1-\alpha}\sin\left(\alpha\frac{\pi}{2}\right)}{1+2(\omega\tau)^{1-\alpha}\sin\left(\alpha\frac{\pi}{2}\right)+(\omega\tau)^{2-2\alpha}}$$

$$\chi_M'' = (\chi_T - \chi_S)\frac{(\omega\tau)^{1-\alpha}\cos\left(\alpha\frac{\pi}{2}\right)}{1+2(\omega\tau)^{1-\alpha}\sin\left(\alpha\frac{\pi}{2}\right)+(\omega\tau)^{2-2\alpha}}$$

With χ_T the isothermal susceptibility, χ_S the adiabatic susceptibility, τ the relaxation time and α an empiric parameter which describe the distribution of the relaxation time. For SMM with only one relaxation time, α is close to zero. The extended Debye model was applied to fit simultaneously the experimental variations of χ_M' and χ_M'' with the frequency ν of the oscillating field ($\omega = 2\pi\nu$). Typically, only the temperatures for which a maximum on the χ_M'' vs. ν curves, have been considered. The best fitted parameters τ, α, χ_T, χ_S are listed in Tables S7-S8 with the coefficient of determination R^2.

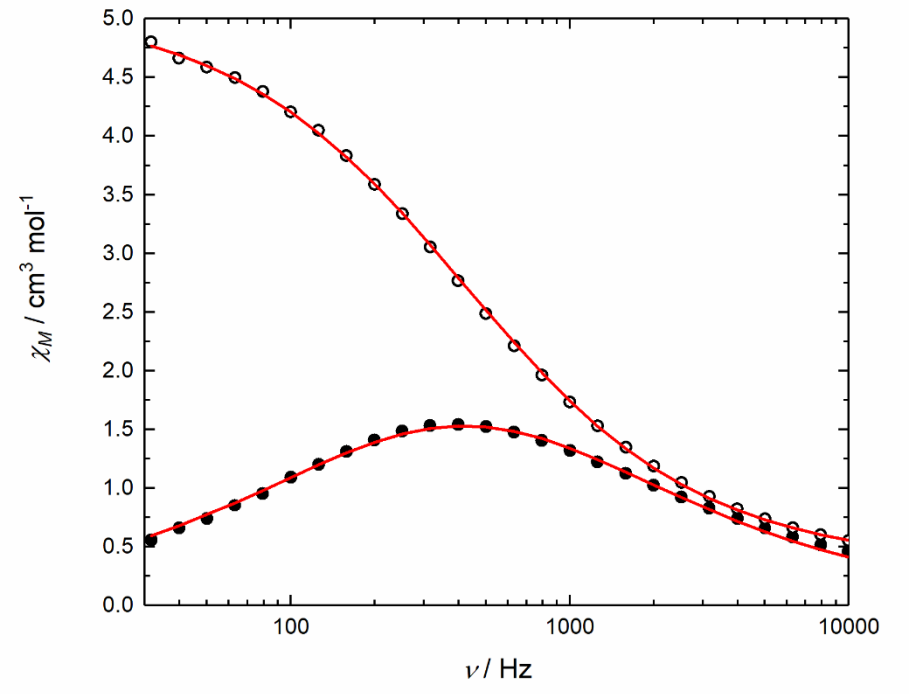

Figure S20. Frequency dependence of the in-phase (χ_M') and out-of-phase (χ_M'') components of the ac susceptibility measured on powder at 2 K and 800 Oe with the best fitted curves (red lines) for **2**.

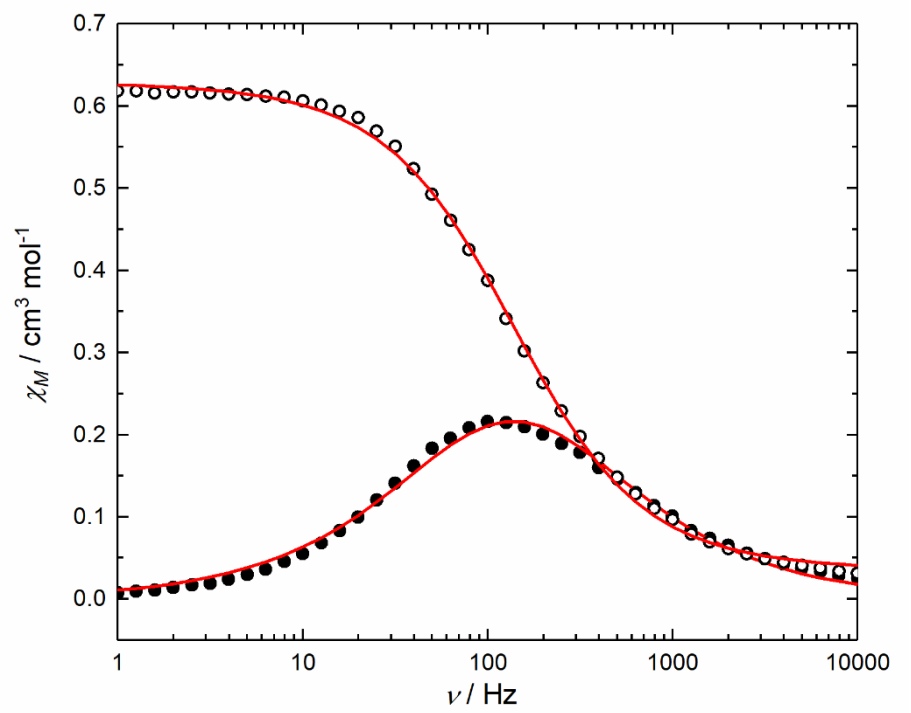

Figure S21. Frequency dependence of the in-phase (χ_M') and out-of-phase (χ_M") components of the ac susceptibility measured on powder at 2 K and 1200 Oe with the best fitted curves (red lines) for **3**.

Extended Debye model used for magnetic susceptibility with two contributions.

$$\chi_M' = \chi_S + (\chi_T - \chi_S)\left\{\frac{\beta\left[1 + (\omega\tau_1)^{1-\alpha_1}\sin\left(\frac{\pi}{2}\alpha_1\right)\right]}{1 + 2(\omega\tau_1)^{1-\alpha_1}\sin\left(\frac{\pi}{2}\alpha_1\right) + (\omega\tau_1)^{2(1-\alpha_1)}} + \frac{(1-\beta)\left[1 + (\omega\tau_2)^{1-\alpha_2}\sin\left(\frac{\pi}{2}\alpha_2\right)\right]}{1 + 2(\omega\tau_2)^{1-\alpha_2}\sin\left(\frac{\pi}{2}\alpha_2\right) + (\omega\tau_2)^{2(1-\alpha_2)}}\right\}$$

$$\chi_M'' = (\chi_T - \chi_S)\left\{\frac{\beta\left[(\omega\tau_1)^{1-\alpha_1}\cos\left(\frac{\pi}{2}\alpha_1\right)\right]}{1 + 2(\omega\tau_1)^{1-\alpha_1}\sin\left(\frac{\pi}{2}\alpha_1\right) + (\omega\tau_1)^{2(1-\alpha_1)}} + \frac{(1-\beta)\left[(\omega\tau_2)^{1-\alpha_2}\cos\left(\frac{\pi}{2}\alpha_2\right)\right]}{1 + 2(\omega\tau_2)^{1-\alpha_2}\sin\left(\frac{\pi}{2}\alpha_2\right) + (\omega\tau_2)^{2(1-\alpha_2)}}\right\}$$

With χ_T the isothermal susceptibility, χ_S the adiabatic susceptibility, τ the relaxation time and α an empiric parameter which describe the distribution of the relaxation time. For SMM with only one relaxing object α is close to zero. The extended Debye model was applied to fit simultaneously the experimental variations of χ_M' and χ_M'' with the frequency ν of the oscillating field ($\omega = 2\pi\nu$). The best fitted parameters τ_1, α_1, χ_{1T}, χ_{1S}, τ_2, α_2, χ_{2T} and χ_{2S} are listed in Tables S5 and S6 with the coefficient of determination R^2. τ_1, α_1, χ_{1T}, χ_{1S} are parameters for the high frequency contribution while τ_2, α_2, χ_{2T} and χ_{2S} are for the low frequency contribution.

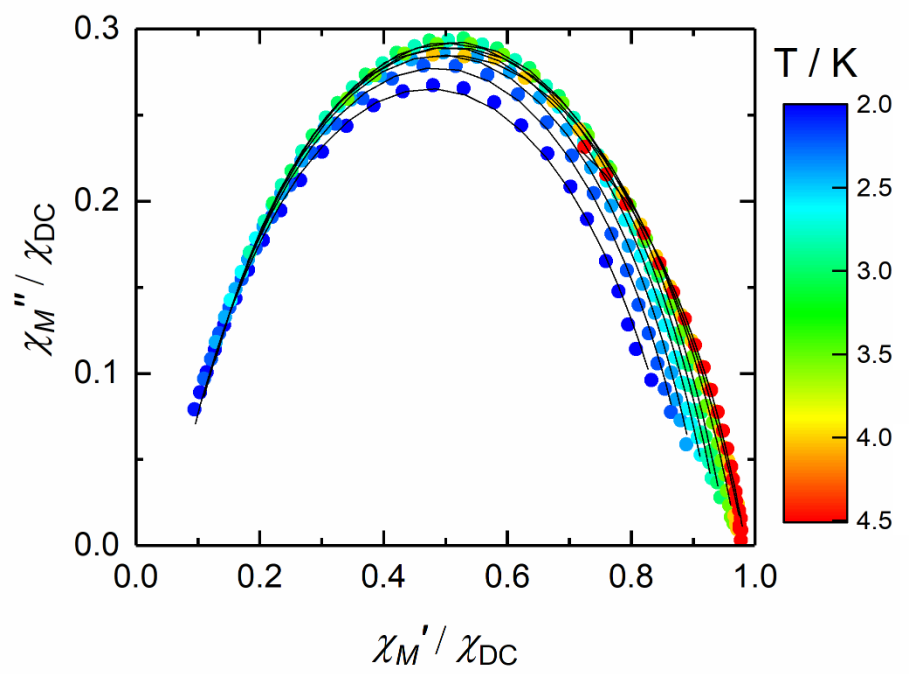

Figure S22. Normalized Argand plot of experimental (colored plots) and fit data (black lines) for **2** under 800 Oe in the temperature range 2-4.5 K.

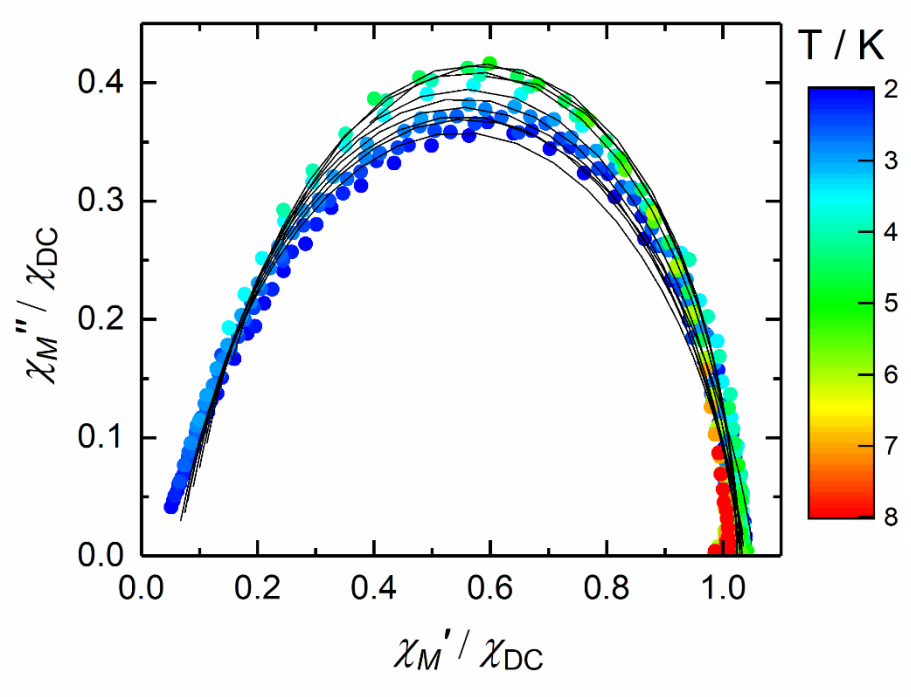

Figure S23. Normalized Argand plot of experimental (colored plots) and fit data (black lines) for **3** under 1200 Oe in the temperature range 2-8 K.

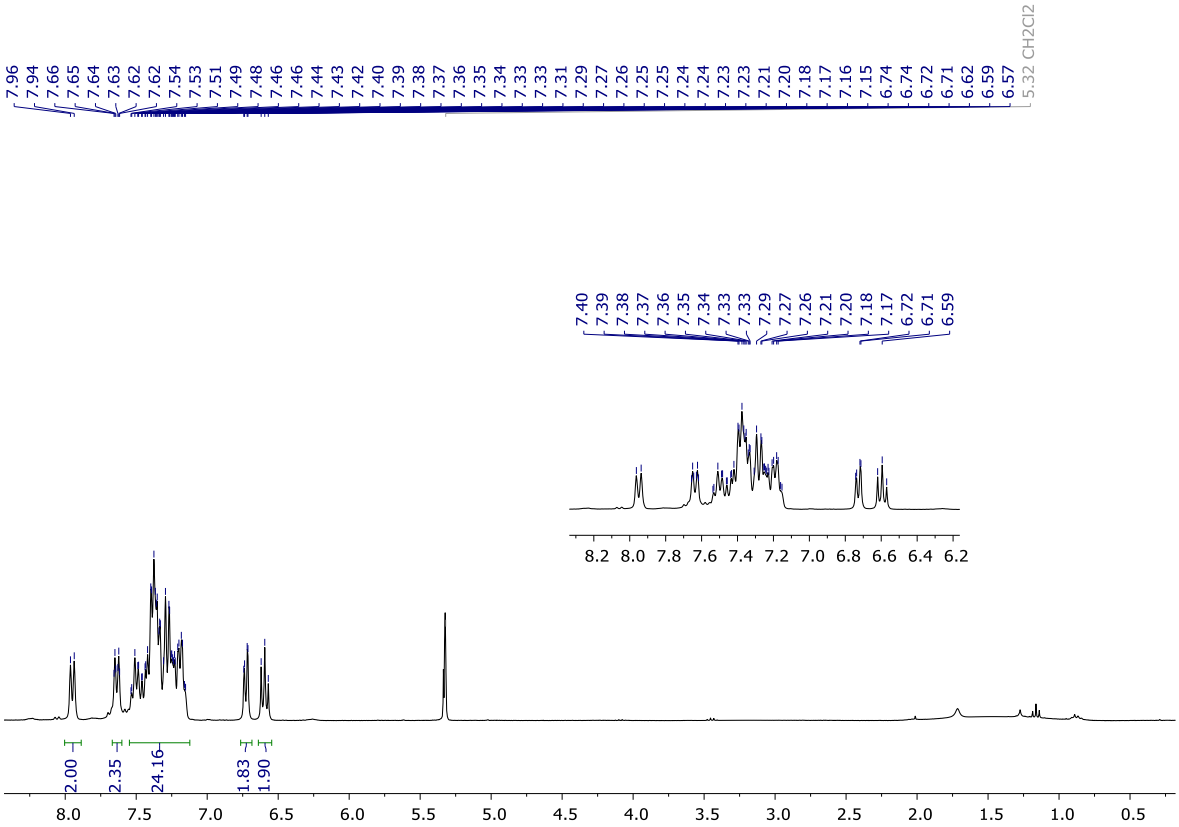

Figure S24: ^{1}H NMR (300 MHz, CD_2Cl_2) of compound **L**.

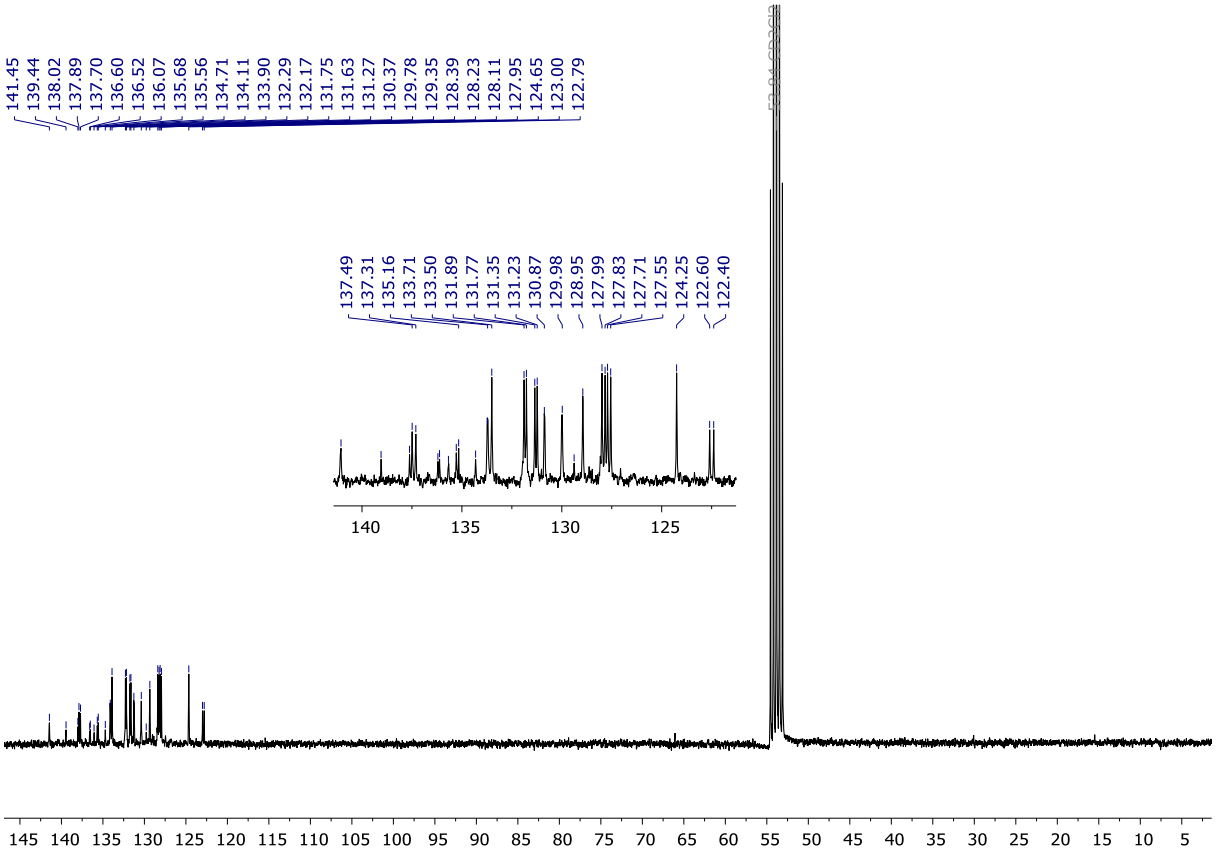

Figure S25: ^{13}CNMR (75 MHz, CD_2Cl_2) of compound **L.**

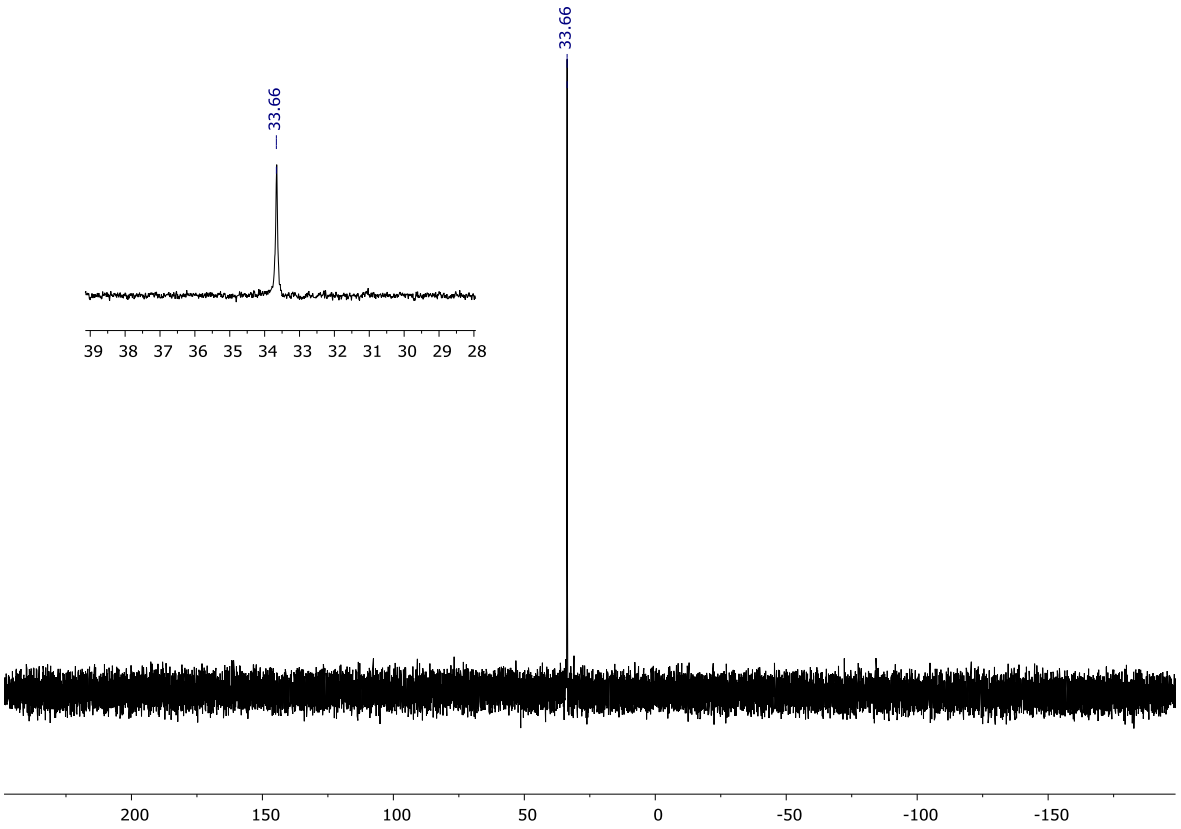

Figure S26: $^{31}P\{^{1}H\}$ NMR (121 MHz, CD_2Cl_2 of compound **L**.

Table S2. X-ray crystallographic data for **2**.

Compound	(**L**)	[{Dy(hfac)$_3$(**L**)}$_3$] (**2**)
Formula	$C_{44}H_{32}O_2P_2$	$C_{59}H_{35}DyF_{18}O_8P_2$
M / g.mol^{-1}	654.63	1438.31
Crystal system	monoclinic	monoclinic
Space group	C2/c	P 2$_1$ /c (N° 14)
Cell parameters	a = 15.250(2) b = 9.2405(17) Å c = 23.112(3) Å β = 94.575(9)	a = 33.429(4) Å b = 13.1260(15) Å c = 40.875(5) Å β = 106.669(4)
Volume / Å^3	3246.5(9)	17182(4)
Z	4	12
T / K	150 K	150 K
2θ range /°	5.16 ≤ 2θ ≤ 55.212	4.16 ≤ 2θ ≤ 55.042
ρ_{calc} / g.cm^{-3}	1,339	1,668
μ / mm^{-1}	0,174	1,474
Number of reflections	12983	117424
Independent reflections	3672	38628
R_{int}	0,0691	0,0435
$Fo^2 > 2\sigma(Fo)^2$	3039	31773
Number of variables	217	2485
R_1, ωR_2	0.0596, 0.1496	0.0757, 0.1641

Table S3. SHAPE analysis of the coordination polyhedra around the trivalent lanthanide centres in **2**.

Dy centre	CShM SAPR-8 (square antiprism D_{4d})	CShM BTPR-8 (biaugmented trigonal prism C_{2v})	CShM TDD-8 (triangular dodecahedron D_{2d})	CShM JBTPR-8 (Biaugmented trigonal prism J_{50})
Dy1	0.190	1.913	2.406	2.239
Dy2	0.213	1.738	2.322	2.190
Dy3	0.132	2.593	1.944	2.486

Boltzmann distribution

The population of each state i ($i = 0,1$) at a given temperature T is calculated according to the following equation

$$\frac{N_i}{N_{tot}} = \frac{\frac{N_i}{N_0}}{\sum_{i=0}^{1}\frac{N_i}{N_0}} = \frac{e^{\frac{E_0-E_i}{k_BT}}}{\sum_{i=0}^{1} e^{\frac{E_0-E_i}{k_BT}}}$$

where k_B is the Boltzmann constant and E_i is the energy of the i state.

Table S4. Temperature variation of the distribution population for the E_i states for **3**.

T / K	N_0/N_{tot}	N_1/N_{tot}	N_2/N_{tot}
298	0.55	0.38	0.07
200	0.62	0.36	0.03
150	0.67	0.32	0.01
100	0.75	0.25	0.00
77	0.81	0.19	0.00
50	0.90	0.10	0.00
25	0.99	0.01	0.00
15	1.00	0.00	0.00
7	1.00	0.00	0.00

Table S5. Fit parameters ($\chi_{T,1}$, χ_S, τ_1, α_1, $\chi_{T,2}$, τ_2 and α_2) with the extended Debye model for the compound **2** at 2 K in the magnetic field range 0-3000 Oe.

H / Oe	$\chi_{T,1}$ / cm^3 mol^{-1}	χ_S / cm^3 mol^{-1}	τ_1 / s	α_1	$\chi_{T,2}$ / cm^3 mol^{-1}	τ_2 / s	α_2	R^2
200	5.84752	3.30923	1.69E-04	0.08979	—	—	—	0.99998
400	5.79080	1.45275	2.43E-04	0.16832	—	—	—	0.99978
600	5.66390	0.86610	3.16E-04	0.20338	—	—	—	0.99985
800	5.51708	0.51422	3.55E-04	0.25815	—	—	—	0.99965
1000	5.32895	0.33593	3.88E-04	0.29501	—	—	—	0.99960
1200	5.13399	0.23881	3.99E-04	0.34220	—	—	—	0.99906
1400	4.76110	0.23498	3.72E-04	0.34056	0.53263	7.43E-02	-0.01846	0.99944
1600	4.45930	0.16786	3.29E-04	0.36394	0.57460	7.48E-02	0.04318	0.99937
1800	4.15478	0.09085	2.72E-04	0.39022	0.59888	7.56E-02	0.08604	0.99924
2000	3.85960	0.00000	2.14E-04	0.41911	0.59756	7.71E-02	0.11585	0.99912
2200	3.51604	0.00000	1.64E-04	0.42808	0.76095	7.83E-02	0.19909	0.99895
2400	3.17988	0.00000	1.21E-04	0.43546	0.94721	8.34E-02	0.27985	0.99871
2600	2.85866	0.00000	8.65E-05	0.44198	1.13316	9.08E-02	0.35243	0.99848
2800	2.55705	0.00000	6.01E-05	0.44535	1.32290	1.02E-01	0.41499	0.99832
3000	2.28594	0.00000	4.17E-05	0.44790	1.49739	1.19E-01	0.46789	0.99838

Table S6. Fit parameters ($\chi_{T,1}$, χ_S, τ_1, α_1, $\chi_{T,2}$, τ_2 and α_2) with the extended Debye model for the compound **3** at 2 K in the magnetic field range 0-3000 Oe.

H / Oe	$\chi_{T,1}$ / cm^3 mol^{-1}	χ_S / cm^3 mol^{-1}	τ_1 / s	α_1	$\chi_{T,2}$ / cm^3 mol^{-1}	τ_2 / s	α_2	R^2
200	0.36045	0.15970	5.16E-04	0.05823	0.42784	2.62E-05	0.27115	0.99984
400	0.63063	0.17824	6.62E-04	0.10520	—	—	—	0.99894
600	0.63379	0.07775	7.97E-04	0.16108	—	—	—	0.99914
800	0.63303	0.05008	9.61E-04	0.17735	—	—	—	0.99919
1000	0.63228	0.03981	1.08E-03	0.18648	—	—	—	0.99915
1200	0.62998	0.03462	1.16E-03	0.19885	—	—	—	0.99915
1400	0.62730	0.03185	1.19E-03	0.20663	—	—	—	0.99922
1600	0.62307	0.03099	1.20E-03	0.20969	—	—	—	0.99919
1800	0.61861	0.02963	1.20E-03	0.21994	—	—	—	0.99917
2000	0.61455	0.02948	1.20E-03	0.22404	—	—	—	0.99912
2200	0.60872	0.02814	1.17E-03	0.23334	—	—	—	0.99932
2400	0.60306	0.02777	1.15E-03	0.24180	—	—	—	0.99930
2600	0.59727	0.02696	1.12E-03	0.24875	—	—	—	0.99926
2800	0.59048	0.02641	1.08E-03	0.25369	—	—	—	0.99937
3000	0.58344	0.02592	1.04E-03	0.25947	—	—	—	0.99941

Table S7. Fit parameters ($\chi_{T,}$, χ_S, τ and α) with the extended Debye model for the compound **2** at 800 Oe in the temperature range 2-4 K.

T / K	χ_T / cm^3 mol^{-1}	χ_S / cm^3 mol^{-1}	τ / s	α	R^2
2	5.15203	0.31412	3.81E-04	0.28174	0.99974
2.2	4.79141	0.31893	2.71E-04	0.26359	0.99978
2.4	4.46430	0.31179	1.93E-04	0.25400	0.99983
2.6	4.18736	0.28829	1.38E-04	0.25390	0.99992
2.8	3.93321	0.26560	9.96E-05	0.25665	0.99994
3	3.70700	0.24136	7.28E-05	0.26215	0.99995
3.5	3.24189	0.15705	3.50E-05	0.28794	0.99990
4	2.87534	0.09150	1.82E-05	0.31368	0.99994

Table S8. Fit parameters (χ_T, χ_S, τ and α) with the extended Debye model for the compound **3** at 1200 Oe in the temperature range 2-5.5 K.

T / K	χ_T / cm^3 mol^{-1}	χ_S / cm^3 mol^{-1}	τ / s	α	R^2
2	0.62955	0.03450	1.15E-03	0.19861	0.99914
2.2	0.57945	0.03421	8.40E-04	0.18484	0.99910
2.4	0.52621	0.03273	5.64E-04	0.16899	0.99932
2.6	0.48480	0.03368	3.94E-04	0.14786	0.99934
2.8	0.44898	0.03411	2.77E-04	0.13105	0.99940
3	0.41968	0.03439	1.99E-04	0.11660	0.99954
3.5	0.36090	0.03595	9.39E-05	0.08105	0.99954
4	0.31637	0.03883	4.82E-05	0.05195	0.99962
4.5	0.28100	0.04412	2.72E-05	0.02475	0.99953
5	0.25346	0.04595	1.65E-05	0.02040	0.99973
5.5	0.23096	0.04931	1.06E-05	0.02013	0.99977